HHS Public Access

Author manuscript

Sci Transl Med. Author manuscript; available in PMC 2022 February 17.

Published in final edited form as:

Sci Transl Med. 2021 February 17; 13(581): . doi:10.1126/scitranslmed.abd7522.

APOE immunotherapy reduces cerebral amyloid angiopathy and amyloid plaques while improving cerebrovascular function

Monica Xiong[1,2], **Hong Jiang**[1], **Javier Remolina Serrano**[1], **Ernesto R. Gonzales**[1], **Chao Wang**[1], **Maud Gratuze**[1], **Rosa Hoyle**[1], **Nga Bien-Ly**[4], **Adam P. Silverman**[5], **Patrick M. Sullivan**[6], **Ryan J. Watts**[4], **Jason D. Ulrich**[1], **Gregory J. Zipfel**[3], **David M. Holtzman**[1,*]

[1]Department of Neurology, Hope Center for Neurological Disorders, Charles F. and Joanne Knight Alzheimer's Disease Research Center, Washington University School of Medicine, St. Louis, MO, 63110, USA

[2]Division of Biology & Biomedical Sciences (DBBS), Washington University School of Medicine, St. Louis, MO, 63110, USA

[3]Department of Neurosurgery, Washington University School of Medicine, St. Louis, MO, 63110, USA

[4]Denali Therapeutics, South San Francisco, CA, 94080, USA

[5]Codexis, Redwood City, CA, 94063, USA

[6]Department of Medicine, Duke University Medical Center, Durham, NC, 27710, USA

Abstract

The ε4 allele of the apolipoprotein E (*APOE*) gene is the strongest genetic risk factor for late-onset Alzheimer Disease (AD) and greatly influences the development of amyloid-β (Aβ) pathology. Our current study investigated the potential therapeutic effects of the anti-human APOE antibody HAE-4, which selectively recognizes human APOE that is co-deposited with Aβ in cerebral amyloid angiopathy (CAA) and parenchymal amyloid pathology. Additionally, we tested whether HAE-4 provoked brain hemorrhages, a component of Amyloid-Related Imaging Abnormalities (ARIA). ARIA is an adverse effect secondary to treatment with anti-Aβ antibodies that can occur in blood vessels with CAA. We utilized 5XFAD mice expressing human *APOE4*$^{+/+}$

*For correspondence contact David M. Holtzman (holtzman@wustl.edu).

Author contributions

D.M.H., M.X., R.J.W., N.B.L., and A.P.S. conceived the study. M.X. and D.M.H. designed the study. M.X., D.M.H., and J.D.U. analyzed the data. H.J. produced HAE-4 and control IgG. N.B.L., A.P.S., and R.J.W., and provided chimeric Aducanumab. M.X. performed most of the experiments, assisted by J.R.S., C.W., M.G., and R.H. M.X. and E.R.G. performed the vessel function study with technical advice and funding support from G.J.Z. P.M.S. provided the *APOE4* KI mice. M.X. and D.M.H. wrote the manuscript with input from all co-authors.

Competing interests

D.M.H. and H.J. are listed as inventors on US patent application #20190270794 entitled "Anti-APOE antibodies" from Washington University on APOE antibodies. N.B.L and R.J.W. are employees at Denali. A.P.S. is an employee of Codexis but conducted this work at Denali. D.M.H. co-founded and is on the scientific advisory board of C2N Diagnostics. D.M.H. is on the scientific advisory board of Denali and consults for Genentech, Merck, and Idorsia. Washington University (D.M.H.) has a sponsored research agreement to work on APOE antibodies from NextCure. All other authors have no competing interests.

Data and materials availability

All materials including HAE-4 are available and can be obtained with a material transfer agreement from Washington University. All data needed to evaluate the conclusions of this paper are listed in the Supplementary Materials.

(5XE4) that have prominent CAA and parenchymal plaque pathology to assess the efficacy of HAE-4 compared to an Aβ antibody that removes parenchymal Aβ but increases ARIA in humans. In chronically-treated 5XE4 mice, HAE-4 reduced Aβ deposition including CAA compared to control IgG, whereas the anti-Aβ antibody had no effect on CAA. Furthermore, the anti-Aβ antibody exacerbated microhemorrhage severity, which highly correlated with reactive astrocytes surrounding CAA. In contrast, HAE-4 did not stimulate microhemorrhages and instead rescued CAA-induced cerebrovascular dysfunction in leptomeningeal arteries in vivo. HAE-4 not only reduced amyloid but also dampened reactive microglial, astrocytic, and proinflammatory-associated genes in the cortex. These results suggest that targeting APOE in the core of both CAA and plaques could ameliorate amyloid pathology while protecting cerebrovascular integrity and function.

One sentence summary:

Targeting APOE using an anti-APOE antibody ameliorates amyloid pathology while protecting cerebrovascular integrity and function.

Introduction

Therapeutic approaches using passive immunotherapy targeting amyloid-β (Aβ) are at the forefront of disease-modifying strategies to treat Alzheimer Disease (AD). Aβ, which deposits in the brain parenchyma as amyloid plaques and in cerebrovasculature as cerebral amyloid angiopathy (CAA), begins to accumulate 15–20 years before cognitive impairment due to AD (1), emphasizing the need for a treatment that is both effective and safe to administer chronically. One potential impediment for anti-Aβ antibodies that successfully remove amyloid in the brain is the manifestation of Amyloid-Related Imaging Abnormalities (ARIA) as ARIA-E (edema) or ARIA-H (hemorrhage), which occurs more frequently in patients who are *APOE* ε4 carriers or receiving high doses of Aβ antibody (2). Some individuals with ARIA become symptomatic with headaches, confusion, and neuropsychiatric symptoms (2). Although the mechanism for ARIA is unclear, Aβ antibody-induced microhemorrhages are associated with CAA (3–6). ARIA is as an adverse effect secondary to treatment with anti-Aβ antibodies targeting aggregated Aβ (7–9) and manifests in the human brain as edema or microhemorrhages that can occur in blood vessels with CAA. Most but not all patients in recent trials on anti-Aβ antibodies who develop ARIA can ultimately remain on the antibodies with dose adjustments (10, 11). However, since CAA is almost universally detected in AD patients (12), Aβ removal with avoidance of ARIA would be greatly preferable.

Although Aβ is the main constituent of extracellular amyloid plaques, there are other less abundant constituents including APOE (13, 14). The *APOE4* gene is the strongest genetic risk factor for late-onset AD and exacerbates the development of Aβ pathology through several mechanisms, including affecting Aβ aggregation and clearance (15, 16). Previously, we demonstrated that passive immunotherapy targeting mouse APOE or human APOE4 reduced Aβ pathology in mice with parenchymal amyloidosis (17–19). Specifically, our anti-human APOE antibody (HAE-4) recognizes poorly-lipidated human APOE only present in amyloid plaques (19).

To recapitulate both the vascular and parenchymal Aβ pathology found in AD human brains, we utilized an animal model that deposits Aβ mostly in the form of CAA but also in the brain parenchyma. Our goal was to determine if HAE-4 treatment could decrease CAA pathology and subsequently improve vessel function without eliciting adverse effects. We compared the treatment effects of HAE-4 against chimeric Aducanumab (chi-Adu), a monoclonal antibody that has shown the ability to remove plaques by binding oligomeric/fibrillar Aβ and induced ARIA in clinical trials (9). We also investigated the mechanisms of action of an APOE antibody and an Aβ antibody, which are largely unknown particularly in the context of CAA.

Results

Anti-human APOE antibody HAE-4 reduces CAA and parenchymal Aβ plaques

First, we validated the efficacy of chi-Adu containing the human variable heavy and light chain sequences of Aducanumab and a mouse IgG2ab Fc domain. Chi-Adu significantly reduced Aβ plaques compared to control IgG in 3.5-month-old 5XFAD (line 6799) mice, which develop aggressive Aβ parenchymal plaques beginning at 2-months-of-age (Fig. S1A: $P < 0.0001$; Fig. S1B: $P < 0.001$). For all further experiments, we used 5XFAD (line 7031) transgenic mice expressing human *APOE4*$^{+/+}$ (5XE4) that exhibit robust CAA starting at 6-months-of-age (20). To assess the efficacy of HAE-4 compared to chi-Adu, we chronically treated 5XE4 mice after CAA and plaque onset from 8- to 10-months-of-age for 8 weeks with weekly intraperitoneal (i.p.) injections at 50 mg/kg (Fig. 1A). HAE-4 significantly reduced Aβ staining (HJ3.4B^{+}; Fig. 1B–E, $P < 0.05$) and fibrillar (Thioflavin-S, ThioS^{+}; Fig. 1F–I, $P < 0.05$) parenchymal and vascular plaques compared to control IgG. HAE-4 reduced both small and large parenchymal Aβ plaques (Fig. S2, $P < 0.05$). There were no sex-dependent differences in Aβ plaque load in response to antibody administrations (Fig. S3A–F), but there was a significant treatment effect (Fig. S3A–E, $P < 0.05$). We also assessed the Aβ concentrations from guanidine-soluble (“insoluble”) fractions of bulk cortical or forebrain vasculature extracts (Fig. 1J–O). HAE-4 significantly reduced insoluble bulk cortical $Aβ_{42}$ (Fig. 1K, $P < 0.01$) and insoluble vascular $Aβ_{40}$ and $Aβ_{42}$ (Fig. 1N, O, $P < 0.05$) compared to chi-Adu but not compared to control IgG (Fig. 1K: $P = 0.09$; Fig. 1N, O: $P = 0.08$). Thus, not only did HAE-4 reduce parenchymal plaques consistent with our previous findings (19), but HAE-4 also decreased CAA and exhibited higher efficacy compared to chi-Adu in a mouse model with prominent CAA.

Chi-Adu but not HAE-4 exacerbates CAA-related microhemorrhages

The pathogenic mechanism underlying ARIA is unclear. One hypothesis is that focal, prolonged inflammation resulting from Aβ antibodies targeting of CAA impairs vascular integrity, leading to microhemorrhages or ARIA (6, 21). Given that HAE-4 is selective for non-lipidated APOE, a small component of the material in ThioS^{+} or X34^{+} dense core plaques and CAA, we hypothesized that HAE-4 would be involved in microglial-mediated Aβ removal but induce less prolonged inflammation compared to chi-Adu. This is because whereas HAE-4 favors dense core fibrillar plaques, chi-Adu binds abundantly to both diffuse and fibrillar plaques in tissue from 5XE4 mice and human CAA and AD (Fig. 2, Table S1) and might have less effective CAA clearance.

To assess for CAA-linked microhemorrhages, we stained brains with Perl's Prussian blue dye, which identifies hemosiderin deposits indicative of prior hemorrhages (Fig. 3A). Whereas HAE-4 did not produce additional antibody-induced microhemorrhages relative to control IgG, chi-Adu exacerbated microhemorrhage severity by increasing the frequency of varying sizes of microbleeds (Fig. 3B–D, $P < 0.05$), recapitulating findings of increased ARIA after Aducanumab treatment in recent clinical trials (9). No sex differences in microhemorrhage incidence were observed among treatment groups (Fig. S3).

HAE-4 restores vascular function to CAA-laden pial arteries

Chronic treatment with HAE-4 reduced parenchymal Aβ plaques and CAA without vascular complications. These results prompted us to ask whether HAE-4-mediated CAA reduction could provide a favorable milieu to rescue cerebrovasculature dysfunction which is caused by CAA (22). In 12-month-old 5XE4 mice treated with control IgG, HAE-4, or chi-Adu for 8 weeks (50 mg/kg, i.p., weekly), we assessed vascular reactivity to vasodilatory pharmacological and physiological agents in leptomeningeal arteries (Fig. 4A). We evaluated vasodilation in vessels with comparable diameters and amount of CAA to dissociate the antibody treatment effect on vasodilation from amyloid removal (Fig. S4). Application of the endothelium-dependent vasodilator acetylcholine (ACH) resulted in significantly improved responses in vessel segments with lower (<50%) and higher (>50%) CAA burden after HAE-4 treatment, nearly restoring vasoreactivity to those of CAA-free, non-transgenic controls (Fig. 4B, C, $P < 0.05$). Vessels with less CAA were expected to retain more function in response to stimuli (22). S-nitro-*N*-acetyl-*DL*-penicillamine (SNAP), a nitric oxide donor that directly relaxes smooth muscle cells was assessed. There were no differences between the 5XE4 mice in the treatment versus control groups (Fig. 4D).. CO_2 challenge using hypercapnia in HAE-4-treated mice also resulted in improved vasodilation compared to control IgG in vessels with lower CAA burden (Fig. 4E, $P < 0.01$). Blood gases collected at normocapnia (baseline) and hypercapnia were not different between groups (Table S2). These results concur with reports of improved vascular function associated with vascular Aβ removal (23). Together, we demonstrated that HAE-4, in addition to not exacerbating CAA-related microhemorrhages, also protected vessel integrity by restoring function to certain cells of the neurovascular unit that are often compromised in CAA (24, 25).

HAE-4 acutely upregulates proinflammatory genes that are mitigated chronically

Amyloid removal by HAE-4 and chi-Adu has been reported to be facilitated by enhanced microglial recruitment to parenchymal plaques (9, 19). In a model with CAA, we hypothesized that chi-Adu engagement with amyloid in vessels without effective clearance may stimulate increased glial-associated inflammation surrounding vessels resulting in increased hemorrhaging events. To capture acute gene expression changes over a shorter timeframe without bias from substantial plaque removal, we injected 11-month 5XE4 mice with abundant existing CAA/plaques 4 times across 10 days with HAE-4, chi-Adu, or control IgG (50 mg/kg, i.p.; Fig. 5A). In this subacute treatment paradigm, there was not a significant reduction of $X34^+$ fibrillar plaques although there was a trend with HAE-4 (Fig. 5B–D, Fig. 5B: $P = 0.10$; Fig. 5D: $P = 0.12$). Next, we evaluated the amount of reactive microglia using CD45. HAE-4 treatment elicited a large increase in $CD45^+$ microglial

staining that was stronger than the effect by chi-Adu (Fig. 5E, F, $P < 0.01$). Furthermore, HAE-4 upregulated both homeostatic (*Cx3cr1, Tmem119, P2ry12)* and reactive or disease-associated (*Trem2*) (26, 27) microglial genes in the cortex, whereas chi-Adu significantly increased homeostatic (*P2ry12*) microglial gene expression (Fig. 5G, $P < 0.05$). Both treatments stimulated reactive astrocytes, with chi-Adu upregulating more astrocytic genes (Fig. 5G, $P < 0.05$). Furthermore, acute HAE-4 and chi-Adu treatments also increased certain proinflammatory cytokine genes likely released by reactive microglia, astrocytes, or vascular cells (Fig. 5G, $P < 0.05$). The striking upregulation of gliosis after acute treatment prompted us to also assess the effects in chronically-treated mice. In 10-month-old 5XE4 mice treated with HAE-4, chi-Adu, and control IgG for 2 months, we observed that HAE-4 downregulated certain genes expressed in microglia, astrocytes, and proinflammatory cytokines, likely from the reduction of plaque-associated gliosis (Fig. 6A, $P < 0.05$). Moreover, after acute HAE-4 treatment, there was also an initial upregulation of certain genes related to the vasculature and reactive oxygen species that were ameliorated after chronic treatment (Fig. S5, $P < 0.05$). Collectively, these results suggest that in HAE-4-treated mice, there was an initial upregulation of inflammatory genes associated with microglia, astrocytes, and vascular cells that was mitigated after chronic treatment and plaque removal, whereas chi-Adu showed an initial inflammatory response that was sustained chronically.

Antibody treatments stimulate differential glial responses to CAA and plaques

Our gene expression study investigated global mRNA changes in 5XE4 cortex, but any specific changes on a per plaque basis may be masked by bulk qPCR. When we assessed glia at the protein/plaque level using immunofluorescent staining, there was robust $Iba1^+$ microglia colocalization with both CAA and parenchymal plaques in mice treated acutely or chronically with HAE-4 (Fig. 6B, D–F; Fig. S6A–C, $P < 0.05$). In contrast, there was a significant increase in $GFAP^+$ astrocytes colocalized with CAA only in chi-Adu-treated mice in the chronic treatment paradigms (Fig. 6C, H–J, $P < 0.05$) but not after subacute treatment (Fig. S6D–F, Fig. S6F: $P = 0.07$). We then assessed whether glial clustering around CAA was linked to microhemorrhages. Whereas the amount of $Iba1^+$ microglia surrounding CAA did not correlate with microhemorrhage number (Fig. 6G, $P > 0.05$), the amount of $GFAP^+$ astrocytes in the immediate vicinity of CAA strongly correlated with microhemorrhage incidence but only in the chi-Adu group (Fig. 6K, $P < 0.05$). These results suggest that somehow an anti-Aβ but not an anti-APOE antibody differentially stimulates a chronic astrocyte reactivity around CAA that contributes to CAA-associated microhemorrhages.

Discussion

Over the past 25 years, the amyloid hypothesis has gained traction as one of the main contributors for the pathogenesis of AD. Overwhelming evidence from genetic, pathological, and biochemical data implicate cerebral Aβ accumulation as the initiator of AD in the long preclinical phase which is followed by tau pathology in the early clinical phase. Numerous anti-Aβ antibodies have been developed and engineered to recognize oligomerized/aggregated forms of Aβ. Some of these antibodies such as Aducanumab, Gantanerumab, and BAN-2401 can remove brain amyloid, improve downstream markers of degeneration such as

CSF tau, p-tau, and NfL, and possibly slow cognitive decline in clinical trials. Although promising, these types of Aβ antibodies have all resulted in ARIA, an adverse effect that occurs in association with CAA resulting in brain edema and hemorrhages. Multiple theories have been postulated for the pathogenesis of ARIA, but the underlying mechanism is still unknown. ARIA is exacerbated in patients who are *APOE4* carriers or receiving higher Aβ antibody dosing (2). Because *APOE4* is the greatest genetic risk factor for sporadic AD and CAA and the APOE protein is deposited within Aβ plaques and CAA, various therapeutic strategies have targeted *APOE4* and exhibited success in reducing parenchymal Aβ plaque burden in mice (see (28) for review). Our lab generated antibodies against human APOE4 (HAE-4) to remove Aβ plaques and facilitate Aβ clearance. Here, we aimed to answer the following questions: [1] Can HAE-4 also reduce CAA, a comorbid neuropathological finding among most AD patients, by targeting a specific form of APOE after plaque and CAA onset? [2] Does HAE-4 exacerbate microhemorrhage severity compared to an Aβ antibody – why or why not? [3] Does HAE-4 treatment have downstream benefits on inflammatory gene expression or vascular function in CAA-laden vessels? [4] Are there fundamental mechanistic differences between the effects of an APOE antibody versus an Aβ antibody?

In this study, we report that HAE-4 has a synergistic effect in reducing CAA and Aβ parenchymal plaques while neutralizing Aβ-mediated vascular toxicity even after the onset of plaque deposition (see schematic model in Fig. S7). HAE-4 specifically binds to poorly-lipidated APOE in the core of plaques and recruits microglia. We discover here that this form of APOE is also found in CAA. Our previous results show that parenchymal plaque removal is dependent on Fcγ receptor-mediated phagocytosis and clearance of Aβ (19). Here, we showed a baseline expression of activated perivascular microglia surrounding plaques and CAA (29) that increased after HAE-4 treatment. Specifically, HAE-4 enhanced microgliosis around parenchymal plaques and to a lesser extent around CAA, perhaps because APOE is only a small fraction of the protein that is co-deposited along with Aβ in CAA, which accumulates in the smooth muscle basement membrane and then later intercalates between smooth muscle cells. Despite differences in microglial clustering, HAE-4 decreased Aβ deposition in both brain parenchyma and vessels. HAE-4 reduced CAA likely by either direct cellular uptake and elimination of Aβ by microglia, or by trafficking less Aβ through the perivascular drainage pathway following parenchymal Aβ removal. In AD and CAA pathogenesis, impaired perivascular clearance potentiates CAA buildup (30), meanwhile HAE-4-mediated removal of vascular Aβ plaques may reverse CAA-induced perivascular drainage complications. Plaque/CAA reductions subsequently were also associated with a decrease of certain global glial and proinflammatory genes. These results might help explain why HAE-4 restored leptomeningeal arterial function even when CAA burden was controlled for. Although certain Aβ antibodies that cause CAA-related hemorrhages or transiently leaky vessels may resolve over time with repeated immunization (10), we show that targeting APOE with HAE-4 did not stimulate adverse vascular effects. In our study, we found that ARIA (measured by microhemorrhages) did not arise from initial upregulated focal inflammation related to antibody target engagement on CAA. Whether the absence of ARIA after HAE-4 treatment is attributed to direct APOE removal or indirect targeting of Aβ in CAA remains to be determined. Overall, our results

indicate that HAE-4-mediated reduction of CAA and plaques by microglia is highly effective and also well-tolerated in mice with pre-existing CAA and Aβ plaques.

To compare the therapeutic effects and mechanisms of our APOE antibody to an Aβ antibody that binds to aggregated Aβ, we produced chi-Adu. Recently in one of two Phase 3 trials, Aducanumab reduced amyloid burden and slowed cognitive decline but induced ARIA (31). Certain Aβ antibodies with Fcγ receptor effector function that target the N-terminus or aggregated forms of Aβ increase the incidence of ARIA in clinical trials (11); whereas, less ARIA was reported with Aβ antibodies without effector function (32) or that prominently bind monomeric versus aggregated Aβ (33, 34). It is noteworthy that although HAE-4 also has a functional Fcγ receptor, repetitive treatment with this APOE antibody did not increase microhemorrhages. This suggests that the occurrence of ARIA results from a fundamentally different mechanism of action between APOE and Aβ antibodies. The original study characterizing Aducanumab revealed substantial removal of Aβ parenchymal plaque but no effect on CAA after chronic treatment (9). Similarly, in our current study, we confirmed that chi-Adu was extremely efficacious in decreasing Aβ accumulation in a parenchymal Aβ plaque mouse model. However, the original study was conducted in mice with minimal CAA and did not assess for microhemorrhages. Because CAA severity is a major risk factor for microhemorrhages, we conducted a follow-up study in mice with robust CAA. In this CAA mouse model, chi-Adu did not reduce parenchymal and vascular plaques despite immunofluorescent staining suggesting abundant binding of chi-Adu to both diffuse and fibrillar CAA and plaque deposits. Although the original study on Aducanumab identified Aβ plaque removal through an Fcγ receptor-mediated mechanism by recruitment of microglia (9), we report here that high CAA load impedes recruitment of reactive microglia after chi-Adu treatment, which may partially explain the lack of treatment efficacy. Interestingly, chi-Adu administration stimulated reactive astrocyte clustering around CAA which correlated with microhemorrhage severity. The chronic reactivity of these $GFAP^+$ astrocytes may lose their normal functions, such as maintenance of the blood-brain barrier, and adopt a disease-associated function that leads to leaky vessels and brain hemorrhages. In our gene expression data, we measured an increase in *Il1a, Tnfa*, and *C1q* cytokines that were described to be released by microglia to induce A1 astrocytes (35) but, in contradiction, we detected little evidence that chi-Adu morphologically stimulated reactive microglia, suggesting these proinflammatory cytokines may originate from another source. The function of these astrocytes and whether they directly cause microhemorrhages or are a result of infiltrating peripheral proteins is currently under investigation. It is also possible that the binding of chi-Adu to widespread Aβ without effective clearance may lock the brain in a sustained state of chronic inflammation that may give rise to ARIA.

In addition to the unanswered questions of our study described above, there are several other limitations to our study. First, although the 5XE4 mouse model that we used recapitulates CAA pathology in humans, this model does not capture the full spectrum of AD. 5XE4 mice do not develop intracellular tau accumulation and tau-mediated cognitive deficits. Therefore, our findings suggest that HAE-4 is highly effective in the early phase of AD when there is prominent neocortical Aβ but not much tau pathology. However, the effects of HAE-4 on the clinical phase of AD that is also modulated by tau pathology are unknown. Furthermore, microglial activation in the presence of mutated human tau has recently been shown to

exacerbate tauopathy (36). Although HAE-4 does not promote vascular complications, it will be important to understand the effect of HAE-4-induced microgliosis on tauopathy, tau spreading, and tau-mediated neurodegeneration. Second, our study would benefit from testing in mice expressing other *APOE* isoforms, particularly *APOE3,* the most frequent *APOE* allele present in humans. We anticipate that mice expressing APOE3 would also show reductions in Aβ plaque deposition because there is similar binding affinity of HAE-4 to both APOE3 and APOEE4. However, these mice would need additional characterization before testing because *APOE3* mice have delayed Aβ onset and progression and much less CAA compared to *APOE4*-expressing mice (15, 37). Third, although the mechanism for ARIA is still not completely clear, we provide new insights into associations between microhemorrhages and $GFAP^+$ astrocytes around CAA following chi-Adu versus HAE-4 treatments. Other studies have shown increased activation of astrocytes in the presence of CAA (29, 38), which is exacerbated in our study after chi-Adu treatments. A major challenge for determining the significance of these astrocytes to Aβ antibody treatment-induced ARIA is to determine if similar astrocyte activation around CAA occurs in humans following treatment with antibodies to aggregated forms of Aβ. Also, since ARIA generally resolves over time, it may be difficult to capture and understand in human studies. Further studies in mice could be performed by isolating and characterizing vessel-associated astrocytes. Fourth, although astrocytes are the predominant producers of lipidated APOE that are high density lipoprotein (HDL)-like in the central nervous system (CNS), the source of poorly-lipidated APOE found specifically in the core of Aβ plaques is yet to be determined. Recent findings suggest that one potential cellular source of less-lipidated APOE are microglia, which secrete APOE particles in vitro that are smaller and thus less-lipidated compared to the larger HDL-like particles produced by astrocytes (46). Whether poorly-lipidated APOE, secreted by microglia or another cell source, acts as a pathological seed to promote Aβ accumulation or whether APOE is stripped of its lipid particles by another mechanism after being incorporated into insoluble plaques remains unknown. It is known that the lipidation state of APOE strongly influences amyloid pathology in the brain (28, 39, 40). APP transgenic mice deficient in the transporter ATP binding cassette transporter A1 (*Abca1*) gene have decreased lipid associated with APOE along with increased plaque burden, greater percentage of insoluble APOE that is co-deposited with insoluble Aβ (41), and reduced Aβ clearance in *APOE4* mice (42). Meanwhile, overexpression of *Abca1* or treatment with drugs that increase APOE lipidation strongly reduces Aβ plaque deposition in APP transgenic mice (43, 44). In humans, *APOE4* carriers have more lipid-depleted APOE in the CSF compared to non-*APOE4* carriers (45). These data suggest that poorly-lipidated APOE may play a role in seeding Aβ plaques and/or hindering Aβ efflux from the CNS. By targeting poorly-lipidated APOE in the core of plaques in our study, HAE-4 is directly recruiting microglia to Aβ plaques for degradation.

Before an antibody such as HAE-4 can move into clinical trials, it would need to be humanized and tested for safety in other species, such as non-human primates. A critical lesson learned from the negative outcome of some clinical trials using Aβ immunotherapy is to administer treatments as early as possible during amyloid buildup in the preclinical phase to prevent subsequent tau-mediated neurodegeneration and downstream events. To do so, the ideal treatment strategy should be both efficacious and safe to administer chronically. In

addition to no vascular complications even at doses given 5X higher than other anti-Aβ antibodies that have been used in clinical trials, we previously showed that HAE-4 does not bind to circulating (lipidated) APOE, minimizing potential adverse effects on lipid metabolism that are of concern for other therapeutics targeting APOE.

Although several anti-Aβ antibodies including Aducanumab remain promising potential treatments for AD because they are undeniably efficacious in removing Aβ in certain mouse models and the human brain, ARIA is a side effect seen in some individuals that can be problematic. Targeting poorly-lipidated APOE, a subcomponent of both amyloid plaques and CAA, appears to allow for retention of efficacy seen with Aβ antibodies while preventing CAA-related microhemorrhages in a mouse model. Taken together, the therapeutic effects of HAE-4 on amyloid removal and the cerebrovasculature may provide a disease-modifying treatment for AD and CAA.

Materials and Methods

Study Design

The objective of this study was to determine whether HAE-4 could treat CAA and improve vascular function compared to an Aβ antibody that removes amyloid but causes ARIA in human clinical trials. To test this, we utilized transgenic mice with robust CAA that expressed human *APOE4.* These mice were treated from 8 to 10 months of age, an age where plaque deposition was already present to better represent the pre-existing plaque load conditions in clinical trials. From these mice, we analyzed samples by performing qPCR for gene expression, live imaging for vasofunction, ELISA for protein concentrations, and staining on tissue sections for protein load and colocalization. Equal numbers of male and female mice were randomly assigned to each experiment. Power analysis calculations for the studies assessing Aβ removal after 8 weeks used standard algorithms to determine the number of mice needed to see at least a 30% difference between groups and statistical significance. Animal numbers for assessing vascular function and acute effects were based on previous publications (17, 47). Antibody treatment groups were randomly assigned to each group. The following outliers detected by Grubb's test ($P < 0.05$) were excluded: 1) One 10-month-old 5XE4 female mouse treated with HAE-4 in all gene expression analysis after identifying an outlier for at least five measured genes, 2) One 3.5-month-old 5XFAD male mouse treated with chi-Adu in all Aβ pathology analyses after identifying an outlier for two different assays. All data analyses were performed blind to the genotype or treatment of the animals. Each animal represented an individual biological replica. Replication and sample sizes for all experiments are detailed in the figure legends.

Animals

All animal procedures and protocols were approved by the Animal Studies Committee at Washington University School of Medicine. 5XFAD mice (line Tg7031) were originally on a C57/B6 X SJL background (a gift from Dr. Robert Vassar at Northwestern University) (48). Human *APOE4*$^{+/+}$ knock-in mice on a C57BL/6 J background express human APOE4 under control of the native murine *Apoe* gene regulatory sequences (49). 5XFAD and *APOE4*$^{+/+}$ mice were crossed to generate 5XFAD / *APOE4*$^{+/+}$ (5XE4) mice (20). All

subsequent mice were bred on a C57/BL6 J background for at least 10 generations and each study utilized mice bred on the same generation. Age-matched *APOE4*$^{+/+}$ littermates negative for the 5XFAD transgene were used as non-transgenic, wildtype controls. Male 5XFAD mice (line Tg6799) on a C57/B6 X SJL background were purchased from The Jackson Laboratory (34840-JAX). All mice were housed in standard cages under pathogen-free conditions on a normal 12-h light/dark cycle with ad libitum access to food.

Antibody generation

The generation of murine HAE-4 and control IgG was previously described (19). The control IgG recognizes human PLD3 sequences not found in mice. HAE-4 and control IgG are IgG2ab isotype. The protein sequences for chimeric aducanumab (chi-Adu) variable heavy chain and light chain (WO 2016/087944) were codon-optimized, generated as double-stranded DNA fragments (Integrated DNA Technologies), and cloned into expression vectors with mouse IgG2ab and mouse Kappa constant regions, respectively. Recombinant antibody was produced by transient co-transfection of heavy and light chain vectors in Expi293 cells (Thermo Fisher) followed by purification by Protein G chromatography. All materials including HAE-4 produced by the Holtzman lab can be obtained by academic investigators with a Material Transfer Agreement from Washington University.

Tissue harvesting

Mice were anesthetized with pentobarbital (200 mg/kg, i.p.) and transcardially perfused with cold PBS containing 0.3% heparin. One hemibrain was dissected, flash-frozen on dry ice, and stored at −80 °C for biochemical analyses. The other hemibrain was fixed for 24 – 48 hours in 4% paraformaldehyde and cryoprotected in 30% sucrose at 4 °C.

Immunofluorescence

The staining protocol was performed at room temperature and on a shaker unless otherwise noted. The primary antibodies used were: hamster anti-CD31 for endothelial cells (Sigma-Aldrich, MAB1398Z, 1:200), rabbit anti-lba1 for microglia (Wako, 019-19741, 1:5000), biotinylated anti-GFAP for astrocytes (Sigma-Aldrich, MAB3402B, 1:1000), HAE-4 for poorly lipidated APOE (produced in-house, 20 μg/mL), chi-Adu for aggregated Aβ (produced in-house, 20 μg/mL), HJ3.4 conjugated to 488 (produced in-house, 1:500), HJ3.4 conjugated to biotin (produced in-house, 2 μg/mL) accompanied by the following secondary antibodies: Goat anti-hamster Alex Fluor 488 (Jackson ImmunoResearch, 127-545-160, 1:500), donkey anti-rabbit Alexa Fluor 568 (Invitrogen, A10042, 1:1000), Streptavidin Alex Fluor 647 (Invitrogen, S21374, 1:1000), biotin goat anti-mouse IgG (Jackson ImmunoResearch, 115-067-003, 1:2000). The fluorescent dyes used were: Thioflavin S (ThioS, Sigma-Aldrich, T1892, 0.025%), X34 dye (Sigma-Aldrich, SML1954, 1:1000), TOPRO3 for nuclei (Invitrogen, T3605, 1:1000). *Fixed tissue.* Free-floating brain tissue sections were rinsed (3 X 5 min) and permeabilized in 0.25% triton-X-100 in TBS (TBS-X) for 30 min. Sections were then incubated in X34 dye that was prepared in X34 buffer (40% ethanol in TBS) for 30 min. The tissue sections were de-stained with X34 buffer (3 X 2 min) and TBS (3 X 5 min). If primary antibodies were used, slices were then blocked in 3% donkey or goat serum in TBS-X before incubating overnight in primary antibodies with 1% serum in TBS-X at 4 °C. The following day, tissue sections were rinsed (3 X 5 min) and

incubated for 1 hour in secondary antibody in TBS. After washing, brain sections were mounted on slides and coverslipped with Fluoromount-G Mounting Medium (Invitrogen, 00-4958-02) and stored at 4 °C. If X34 was the only stain, images were captured on the Nanozoomer slide scanner. All other images were captured on the Nikon A1R$^+$ confocal microscope. ***Unfixed tissue.*** To preserve the sensitive antigen recognized by HAE-4 for certain experiments, unfixed tissue sections were prepared. ***Unfixed mouse brain sections.*** Immediately after transcardial perfusion and brain extraction, brain hemispheres were snapfrozen in 2-methylbutane (Sigma-Aldrich, 320404) for 1 min before stored at −80 °C. Brains were then sectioned on a Leica CM 1950 cryostat at 20 μm, mounted on Superfrost Plus Microscope Slides (Fisher Scientific), and stored at −20 °C until use. ***Human staining.*** All participants gave prospective pre-mortem written consent for their brains to be banked and used for research. Unfixed human cortical tissue sections (50 μm) were pre-mounted on slides and treated with 50 mM sodium citrate buffer in 0.05% Tween (pH 6.0) at 95 °C for 30 min. Staining proceeded as previously described. Images of unfixed mouse and human brain tissue were captured using the Cytation 5 imager at 4× magnification with image stitching (BioTek). ***Isolated vessels.*** 50 μL of 1 mL resuspended isolated cerebrovasculature in 0.5% BSA in HBSS were dried on slides. Prior to staining, slides with unfixed tissue or vessels were returned to room temperature and promptly fixed in chilled 100% methanol for 10 min. Tissue staining proceeded as described above.

Microhemorrhage analysis

20–21 equally spaced sections (bregma 2.9 to −3.5) were pre-mounted on glass slides before staining. Slides were first stained for vascular bleeds marked by hemosiderin deposits by incubating in 2% potassium ferrocyanide (Sigma-Aldrich, P3289) in 2% hydrochloric acid for 30 min. Next, slides were immersed for 10 min in 0.025% Thioflavin S (ThioS, Sigma-Aldrich, T1892) prepared in 50% ethanol in TBS, and subsequently rinsed in 50% ethanol in TBS (2 X 10 min) and TBS (3 X 5 min) before coverslipped with Fluoromount-G. Slides were imaged with Nanozoomer slide scanner at 40x. Microhemorrhages were manually traced using NDP.View2 software for calculations of microhemorrhage number per brain section and size per microhemorrhage. Analyses and tracings were completed while blind to treatment.

Statistical Analysis

GraphPad Prism 8.0.2 was used to perform all statistical analyses. Data are presented as mean ± SEM. No other statistical comparisons were significant unless otherwise noted. Gaussian distribution of data was first checked with the Anderson-Darling, D'Agostino & Pearson, and Shapiro–Wilk normality tests. Statistical significance between two groups with normally distributed data were calculated using a student's *t*-test (two-tailed). For three or more groups, one-way analysis of variance (ANOVA) followed by Tukey's post hoc test or Dunnett's post hoc test was used to determine statistical significance. If data were not normally distributed, a Kruskal-Wallis test with Dunn's multiple comparisons was performed instead. In studies with multiple groups and two or more factors, a two-way ANOVA with Tukey's post hoc test was calculated for statistical significance.

Supplementary Material

Refer to Web version on PubMed Central for supplementary material.

Acknowledgments

We thank Dr. Robert Vassar for gifting 5XFAD (line 7031) mice; Dr. Aimin Li (deceased) for his work producing chimeric Aducanumab; Drs. Eric Reiman, Geidy Serrano, and Thomas Beach for human brain tissue; Dr. Andrew Johnson for providing technical assistance for the vessel function study; Dr. John Fryer and Aleksandra Wojtas for their detailed vessel isolation protocol; Dr. Fan Liao for technical advice on microhemorrhage and CAA staining and analysis; Dr. Michael Shih and the WUCCI for image analyses consultations; the Animal Surgery Core at the Hope Center for Neurological Disorders for surgery consultations; the Instrument Machine Shop at Washington University for designing and building a custom stereotax; the Genome Technology Access Center in the Department of Genetics at Washington University School of Medicine for help on genomic analysis.

Funding

This work was supported by National Institute of Aging AG062027 (M.X.), NIH 5T32GM008151 (M.X.), NIH AG047644 (D.M.H.), the JPB Foundation (D.M.H.), NIH RF1 NS103276 (G.J.Z.), and 2P30AG019610 (E.R. and T. B.). Images scanned on the NanoZoomer digital pathology system is courtesy of the Hope Center Alafi Neuroimaging Laboratory. Washington University Center for Cellular Imaging (WUCCI) received support from Office of Research Infrastructure Programs (ORIP), a part of the NIH Office of the Director under grant OD021629, for the purchasing of the Nikon A1R^{+} confocal microscope for capturing fluorescent staining.

References and Notes

1. Long JM, Holtzman DM, Alzheimer Disease: An Update on Pathobiology and Treatment Strategies, Cell 179, 312–339 (2019). [PubMed: 31564456]
2. Sperling R, Salloway S, Brooks DJ, Tampieri D, Barakos J, Fox NC, Raskind M, Sabbagh M, Honig LS, Porsteinsson AP, Lieberburg I, Arrighi HM, Morris KA, Lu Y, Liu E, Gregg KM, Brashear HR, Kinney GG, Black R, Grundman M, Amyloid-related imaging abnormalities in patients with Alzheimer's disease treated with bapineuzumab: A retrospective analysis, Lancet Neurol. 11, 241–249 (2012). [PubMed: 22305802]
3. Sperling RA, Jack CR, Black SE, Frosch MP, Greenberg SM, Hyman BT, Scheltens P, Carrillo MC, Thies W, Bednar MM, Black RS, Brashear HR, Grundman M, Siemers ER, Feldman HH, Schindler RJ, Amyloid-related imaging abnormalities in amyloid-modifying therapeutic trials: Recommendations from the Alzheimer's Association Research Roundtable Workgroup, Alzheimer's Dement. 7, 367–385 (2011). [PubMed: 21784348]
4. Wilcock DM, Rojiani A, Rosenthal A, Subbarao S, Freeman MJ, Gordon MN, Morgan D, Passive immunotherapy against Aβ in aged APP-transgenic mice reverses cognitive deficits and depletes parenchymal amyloid deposits in spite of increased vascular amyloid and microhemorrhage, J. Neuroinflammation 1, 1–11 (2004). [PubMed: 15285806]
5. Racke MM, Boone LI, Hepburn DL, Parsadainian M, Bryan MT, Ness DK, Piroozi KS, Jordan WH, Brown DD, Hoffman WP, Holtzman DM, Bales KR, Gitter BD, May PC, Paul SM, DeMattos RB, Exacerbation of cerebral amyloid angiopathy-associated microhemorrhage in amyloid precursor protein transgenic mice by immunotherapy is dependent on antibody recognition of deposited forms of amyloid β, J. Neurosci. 25, 629–636 (2005). [PubMed: 15659599]
6. Pfeifer M, Boncristiano S, Bondolfi L, Stalder A, Deller T, Staufenbiel M, Mathews PM, Jucker M, Cerebral hemorrhage after passive anti-aβ immunotherapy, Science (80-.). 298, 1379–1380 (2002).
7. Ostrowitzki S, Deptula D, Thurfjell L, Barkhof F, Bohrmann B, Brooks DJ, Klunk WE, Ashford E, Yoo K, Xu ZX, Loetscher H, Santarelli L, Mechanism of amyloid removal in patients with Alzheimer disease treated with gantenerumab, Arch. Neurol. 69, 198–207 (2012). [PubMed: 21987394]
8. Salloway S, Sperling R, Fox NC, Blennow K, Klunk W, Raskind M, Sabbagh M, Honig LS, Porsteinsson AP, Ferris S, Reichert M, Ketter N, Nejadnik B, Guenzler V, Miloslavsky M, Wang D, Lu Y, Lull J, Tudor IC, Liu E, Grundman M, Yuen E, Black R, Brashear HR, Two phase 3 trials of

Bapineuzumab in mild-to-moderate Alzheimer's disease, N. Engl. J. Med. 370, 322–333 (2014). [PubMed: 24450891]

9. Sevigny J, Chiao P, Bussière T, Weinreb PH, Williams L, Maier M, Dunstan R, Salloway S, Chen T, Ling Y, O'Gorman J, Qian F, Arastu M, Li M, Chollate S, Brennan MS, Quintero-Monzon O, Scannevin RH, Arnold HM, Engber T, Rhodes K, Ferrero J, Hang Y, Mikulskis A, Grimm J, Hock C, Nitsch RM, Sandrock A, The antibody aducanumab reduces Aβ plaques in Alzheimer's disease, Nature 537, 50–56 (2016). [PubMed: 27582220]
10. Ostrowitzki S, Lasser RA, Dorflinger E, Scheltens P, Barkhof F, Nikolcheva T, Ashford E, Retout S, Hofmann C, Delmar P, Klein G, Andjelkovic M, Dubois B, Boada M, Blennow K, Santarelli L, Fontoura P, A phase III randomized trial of gantenerumab in prodromal Alzheimer's disease, Alzheimer's Res. Ther. 9, 95 (2017). [PubMed: 29221491]
11. Greenberg SM, Bacskai BJ, Hernandez-Guillamon M, Pruzin J, Sperling R, van Veluw SJ, Cerebral amyloid angiopathy and Alzheimer disease — one peptide, two pathways, Nat. Rev. Neurol. 16, 30–42 (2020). [PubMed: 31827267]
12. Attems J, Jellinger KA, Lintner F, Alzheimer's disease pathology influences severity and topographical distribution of cerebral amyloid angiopathy, Acta Neuropathol. 110, 222–231 (2005). [PubMed: 16133541]
13. Namba K, Tomonaga Y, Kawasaki M, Otomo H, Ikeda E, Apolipoprotein E immunoreactivity in cerebral amyloid deposits and neurofibrillary tangles in Alzheimer's disease and kuru plaque amyloid in Creutzfeldt-Jakob disease, Brain Res. 541, 163–166 (1991). [PubMed: 2029618]
14. Xiong F, Ge W, Ma C, Quantitative proteomics reveals distinct composition of amyloid plaques in Alzheimer's disease, Alzheimer's Dement. 15, 429–440 (2019). [PubMed: 30502339]
15. Castellano JM, Kim J, Stewart FR, Jiang H, DeMattos RB, Patterson BW, Fagan AM, Morris JC, Mawuenyega KG, Cruchaga C, Goate AM, Bales KR, Paul SM, Bateman RJ, Holtzman DM, Human apoE Isoforms Differentially Regulate Brain Amyloid-beta Peptide Clearance, Sci. Transl. Med. 3, 89ra57 (2011).
16. Liu C-C, Kanekiyo T, Xu H, Bu G, Apolipoprotein E and Alzheimer disease: risk, mechanisms and therapy, Nat. Rev. Neurol. 9, 106–118 (2013). [PubMed: 23296339]
17. Kim J, Eltorai AEM, Jiang H, Liao F, Verghese PB, Kim J, Stewart FR, Basak JM, Holtzman DM, Anti-apoE immunotherapy inhibits amyloid accumulation in a transgenic mouse model of Aβ amyloidosis, J. Exp. Med. 209, 2149–2156 (2012). [PubMed: 23129750]
18. Liao F, Hori Y, Hudry E, Bauer AQ, Jiang H, Mahan TE, Lefton KB, Zhang TJ, Dearborn JT, Kim J, Culver JP, Betensky R, Wozniak DF, Hyman BT, Holtzman DM, Anti-ApoE antibody given after plaque onset decreases Aβ accumulation and improves brain function in a mouse model of Aβ amyloidosis, J. Neurosci. 34, 7281–7292 (2014). [PubMed: 24849360]
19. Liao F, Li A, Xiong M, Bien-Ly N, Jiang H, Zhang Y, Finn MB, Hoyle R, Keyser J, Lefton KA, Robinson GO, Serrano JR, Silverman AP, Guo JL, Getz J, Henne K, Leyns CEG, Gallardo G, Ulrich JD, Sullivan PM, Lerner EP, Hudry E, Sweeney ZK, Dennis MS, Hyman BT, Watts RJ, Holtzman DM, Targeting of nonlipidated, aggregated apoE with antibodies inhibits amyloid accumulation, J. Clin. Invest. 128, 2144–2155 (2018). [PubMed: 29600961]
20. Liao F, Zhang TJ, Jiang H, Lefton KB, Robinson GO, Vassar R, Sullivan PM, Holtzman DM, Murine versus human apolipoprotein E4: differential facilitation of and co-localization in cerebral amyloid angiopathy and amyloid plaques in APP transgenic mouse models, Acta Neuropathol. Commun. 3, 70 (2015). [PubMed: 26556230]
21. Golde TE, Open questions for Alzheimer's disease immunotherapy, Alzheimer's Res. Ther. 6, 3 (2014). [PubMed: 24393284]
22. Han BH, Zhou ML, Abousaleh F, Brendza RP, Dietrich HH, Koenigsknecht-Talboo J, Cirrito JR, Milner E, Holtzman DM, Zipfel GJ, Cerebrovascular dysfunction in amyloid precursor protein transgenic mice: Contribution of soluble and insoluble amyloid-β peptide, partial restoration via γ-secretase inhibition, J. Neurosci. 28, 13542–13550 (2008). [PubMed: 19074028]
23. Bales KR, O'Neill SM, Pozdnyakov N, Pan F, Caouette D, Pi Y, Wood KM, Volfson D, Cirrito JR, Han BH, Johnson AW, Zipfel GJ, Samad TA, Passive immunotherapy targeting amyloid-β reduces cerebral amyloid angiopathy and improves vascular reactivity, Brain 139, 563–577 (2016). [PubMed: 26493635]

24. Sweeney MD, Sagare AP, Zlokovic BV, Blood-brain barrier breakdown in Alzheimer disease and other neurodegenerative disorders, Nat. Rev. Neurol. 14, 133–150 (2018). [PubMed: 29377008]
25. Iadecola C, The overlap between neurodegenerative and vascular factors in the pathogenesis of dementia, Acta Neuropathol 120, 287–296 (2010). [PubMed: 20623294]
26. Keren-Shaul H, Spinrad A, Weiner A, Matcovitch-Natan O, Dvir-Szternfeld R, Ulland TK, David E, Baruch K, Lara-Astaiso D, Toth B, Itzkovitz S, Colonna M, Schwartz M, Amit I, A Unique Microglia Type Associated with Restricting Development of Alzheimer's Disease, Cell169, 1276–1290.e17 (2017). [PubMed: 28602351]
27. Krasemann S, Madore C, Cialic R, Baufeld C, Calcagno N, El Fatimy R, Beckers L, O'Loughlin E, Xu Y, Fanek Z, Greco DJ, Smith ST, Tweet G, Humulock Z, Zrzavy T, Conde-Sanroman P, Gacias M, Weng Z, Chen H, Tjon E, Mazaheri F, Hartmann K, Madi A, Ulrich JD, Glatzel M, Worthmann A, Heeren J, Budnik B, Lemere C, Ikezu T, Heppner FL, Litvak V, Holtzman DM, Lassmann H, Weiner HL, Ochando J, Haass C, Butovsky O, The TREM2-APOE Pathway Drives the Transcriptional Phenotype of Dysfunctional Microglia in Neurodegenerative Diseases, Immunity 47, 566–581.e9 (2017). [PubMed: 28930663]
28. Yamazaki Y, Zhao N, Caulfield TR, Liu CC, Bu G, Apolipoprotein E and Alzheimer disease: pathobiology and targeting strategies, Nat. Rev. Neurol. 15, 501–518 (2019). [PubMed: 31367008]
29. Herzig MC, Winkler DT, Burgermeister P, Pfeifer M, Kohler E, Schmidt SD, Danner S, Abramowski D, Stürchler-Pierrat C, Bürki K, Van Duinen SG, Maat-Schieman MLC, Staufenbiel M, Mathews PM, Jucker M, Aβ is targeted to the vasculature in a mouse model of hereditary cerebral hemorrhage with amyloidosis, Nat. Neurosci. 7, 954–960 (2004). [PubMed: 15311281]
30. Weller RO, Subash M, Preston SD, Mazanti I, Carare RO, Perivascular drainage of amyloid-β peptides from the brain and its failure in cerebral amyloid angiopathy and Alzheimer's disease, Brain Pathol. 18, 253–266 (2008). [PubMed: 18363936]
31. Haeberlein SB, von Hehn C, Tian Y, Chalkias S, Muralidharan KK, Chen T, Wu S, Li J, Skordos L, Nisenbaum L, Rajagovindan R, Dent G, Harrison K, Nestorov I, Zhu Y, Mallinckrodt C, Sandrock A, in CTAD 2019, (San Diego, CA, 2019), pp. 1–60.
32. Cummings JL, Cohen S, Van Dyck CH, Brody M, Curtis C, Cho W, Ward M, Friesenhahn M, Brunstein F, Quartino A, Honigberg LA, Fuji RN, Clayton D, Mortensen D, Ho A, Paul R, Rabe C, A phase 2 randomized trial of crenezumab in mild to moderate Alzheimer disease, Neurology 90, E1889–E1897 (2018). [PubMed: 29695589]
33. Siemers ER, Sundell KL, Carlson C, Case M, Sethuraman G, Liu-Seifert H, Dowsett SA, Pontecorvo MJ, Dean RA, DeMattos R, Phase 3 solanezumab trials: Secondary outcomes in mild Alzheimer's disease patients, Alzheimer's Dement. 12, 110–120 (2016). [PubMed: 26238576]
34. Leurent C, Goodman JA, Zhang Y, He P, Polimeni JR, Gurol ME, Lindsay M, Frattura L, Sohur US, Viswanathan A, Bednar MM, Smith EE, Greenberg SM, Immunotherapy with ponezumab for probable cerebral amyloid angiopathy, Ann. Clin. Transl. Neurol. 6, 795–806 (2019). [PubMed: 31020004]
35. Liddelow SA, Guttenplan KA, Clarke LE, Bennett FC, Bohlen CJ, Schirmer L, Bennett ML, Münch AE, Chung WS, Peterson TC, Wilton DK, Frouin A, Napier BA, Panicker N, Kumar M, Buckwalter MS, Rowitch DH, Dawson VL, Dawson TM, Stevens B, Barres BA, Neurotoxic reactive astrocytes are induced by activated microglia, Nature 541, 481—487 (2017). [PubMed: 28099414]
36. Shi Y, Manis M, Long J, Wang K, Sullivan PM, Serrano JR, Hoyle R, Holtzman DM, Microglia drive APOE-dependent neurodegeneration in a tauopathy mouse model, J. Exp. Med.216, 2546–2561 (2019). [PubMed: 31601677]
37. Fryer JD, Simmons K, Parsadanian M, Bales KR, Paul SM, Sullivan PM, Holtzman DM, Human apolipoprotein E4 alters the amyloid-β 40:42 ratio and promotes the formation of cerebral amyloid angiopathy in an amyloid precursor protein transgenic model, J. Neurosci. 25, 2803–2810 (2005). [PubMed: 15772340]
38. Taylor X, Cisternas P, You Y, You Y, Xiang S, Marambio Y, Zhang J, Vidal R, Lasagna-Reeves CA, A1 reactive astrocytes and a loss of TREM2 are associated with an early stage of pathology in a mouse model of cerebral amyloid angiopathy, J. Neuroinflammation 17, 223 (2020). [PubMed: 32711525]

39. Liao F, Yoon H, Kim J, Apolipoprotein E metabolism and functions in brain and its role in Alzheimer's disease, Curr. Opin. Lipidol. , 1 (2016).
40. Koldamova R, Fitz NF, Lefterov I, ATP-binding cassette transporter A1: From metabolism to neurodegeneration, Neurobiol. Dis. 72, 13–21 (2014). [PubMed: 24844148]
41. Wahrle SE, Jiang H, Parsadanian M, Hartman RE, Bales KR, Paul SM, Holtzman DM, Deletion of Abca1 increases Aβ deposition in the PDAPP transgenic mouse model of Alzheimer disease, J. Biol. Chem. 280, 43236–43242 (2005). [PubMed: 16207708]
42. Fitz NF, Cronican AA, Saleem M, Fauq AH, Chapman R, Lefterov I, Koldamova R, Abca1 deficiency affects Alzheimer's disease-like phenotype in human ApoE4 but not in ApoE3-targeted replacement mice, J. Neurosci. 32, 13125–13136 (2012). [PubMed: 22993429]
43. Wahrle SE, Jiang H, Parsadanian M, Kim J, Li A, Knoten A, Jain S, Hirsch-Reinshagen V, Wellington CL, Bales KR, Paul SM, Holtzman DM, Overexpression of ABCA1 reduces amyloid deposition in the PDAPP mouse model of Alzheimer disease, J. Clin. Invest. 118, 671–682 (2008). [PubMed: 18202749]
44. Cramer PE, Cirrito JR, Wesson DW, Lee CYD, Karlo JC, Zinn AE, Casali BT, Restivo JL, Goebel WD, James MJ, Brunden KR, Wilson DA, Landreth GE, ApoE-directed therapeutics rapidly clear β-amyloid and reverse deficits in AD mouse models, Science (80-.). 335, 1503–1506 (2012).
45. Hanson AJ, Bayer-Carter JL, Green PS, Montine TJ, Wilkinson CW, Baker LD, Watson GS, Bonner LM, Callaghan M, Leverenz JB, Tsai E, Postupna N, Zhang J, Lampe J, Craft S, Effect of apolipoprotein e genotype and diet on apolipoprotein e lipidation and amyloid peptides randomized clinical trial, JAMA Neurol. 70, 972–980 (2013). [PubMed: 23779114]
46. Huynh TPV, Wang C, Tran AC, Tabor GT, Mahan TE, Francis CM, Finn MB, Spellman R, Manis M, Tanzi RE, Ulrich JD, Holtzman DM, Lack of hepatic apoE does not influence early Aβ deposition: Observations from a new APOE knock-in model, Mol. Neurodegener. 14(2019).
47. Han GJ, Zhou BH, Johnson ML, Singh AW, Liao I, Vellimana F, Nelson AK, Milner JW, Cirrito E, Basak JR, Yoo J, Han M, Zhou BH, Johnson ML, Singh AW, Liao I, Vellimana F, Nelson AK, Milner JW, Cirrito E, J.R., Contribution of reactive oxygen species to cerebral amyloid angiopathy, vasomotor dysfunction, and microhemorrhage in aged Tg2576 mice, Proc. Natl. Acad. Sci. 112, E881–E890 (2015). [PubMed: 25675483]
48. Oakley H, Cole SL, Logan S, Maus E, Shao P, Craft J, Guillozet-Bongaarts A, Ohno M, Disterhoft J, Van Eldik L, Berry R, Vassar R, Intraneuronal β-amyloid aggregates, neurodegeneration, and neuron loss in transgenic mice with five familial Alzheimer's disease mutations: Potential factors in amyloid plaque formation, J. Neurosci. 26, 10129–10140 (2006). [PubMed: 17021169]
49. Sullivan PM, Mezdour H, Aratani Y, Knouff C, Najib J, Reddick RL, Quarfordt SH, Maeda N, Targeted replacement of the mouse apolipoprotein E gene with the common human APOE3 allele enhances diet-induced hypercholesterolemia and atherosclerosis, J. Biol. Chem. 272, 17972–17980 (1997). [PubMed: 9218423]
50. Wojtas AM, Kang SS, Olley BM, Gatherer M, Shinohara M, Lozano PA, Liu CC, Kurti A, Baker KE, Dickson DW, Yue M, Petrucelli L, Bu G, Carare RO, Fryer JD, Loss of clusterin shifts amyloid deposition to the cerebrovasculature via disruption of perivascular drainage pathways, Proc. Natl. Acad. Sci. U. S. A 114, E6962–E6971 (2017). [PubMed: 28701379]
51. Shi Y, Yamada K, Liddelow SA, Smith ST, Zhao L, Luo W, Tsai RM, Spina S, Grinberg LT, Rojas JC, Gallardo G, Wang K, Roh J, Robinson G, Finn MB, Jiang H, Sullivan PM, Baufeld C, Wood MW, Sutphen C, McCue L, Xiong C, Del-Aguila JL, Morris JC, Cruchaga C, Fagan AM, Miller BL, Boxer AL, Seeley WW, Butovsky O, Barres BA, Paul SM, Holtzman DM, ApoE4 markedly exacerbates tau-mediated neurodegeneration in a mouse model of tauopathy, Nature 549, 523–527 (2017). [PubMed: 28959956]

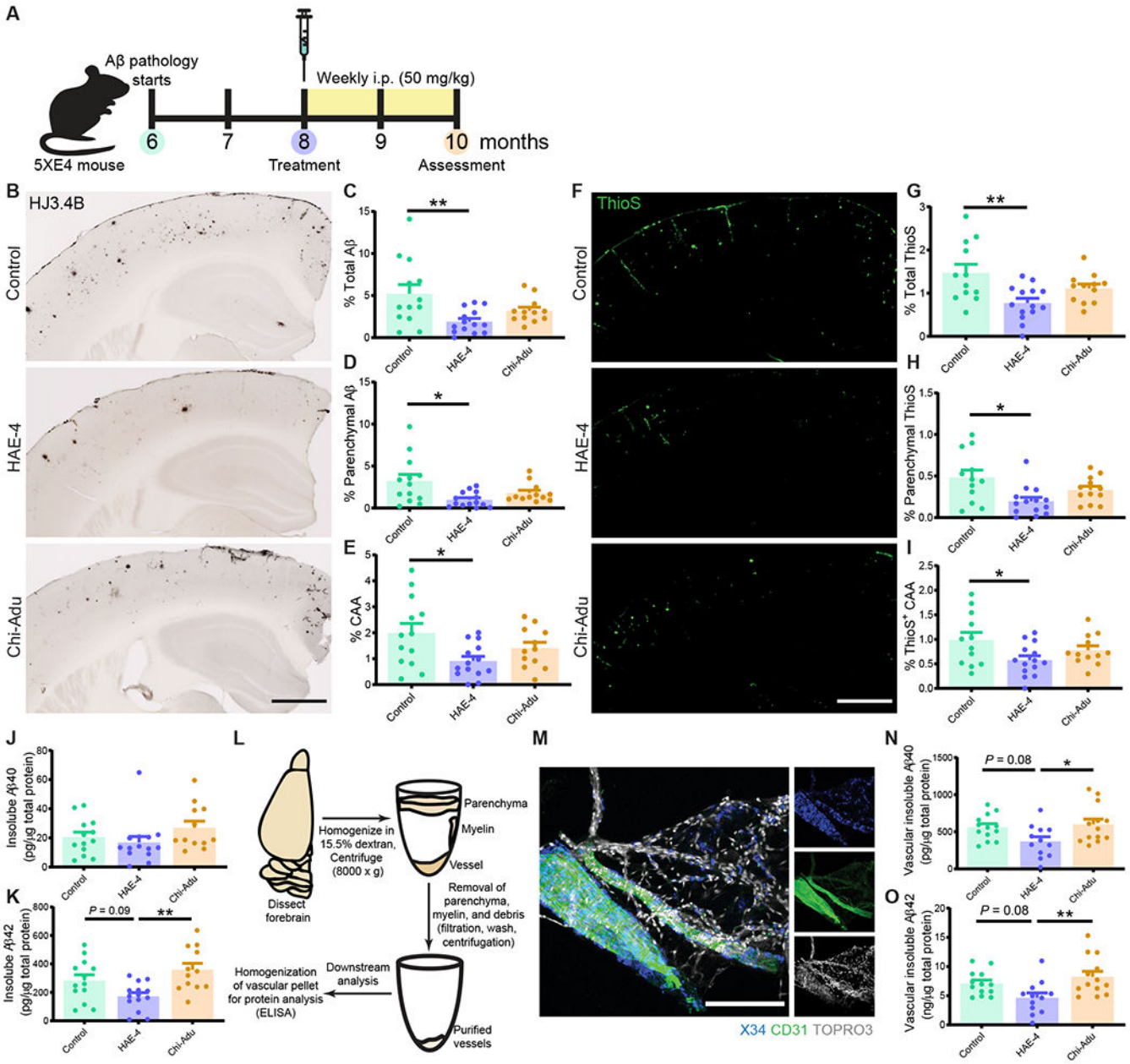

Fig. 1: HAE-4 reduces parenchymal Aβ plaques and CAA in 5XE4 mice.

A, Schematic timeline of antibody treatment in 5XFAD (line 7031) x *APOE4*$^{+/+}$ (5XE4) mice with CAA assessed at 10-months-old. **B–E**, Representative immunostainings of HJ3.4B for mixed pan-Aβ pathology (**B**) and quantification of percent area in cortex of total Aβ (**C**), parenchymal Aβ plaques (**D**), and CAA (**E**). Control IgG, n = 13; HAE-4, n = 14, chi-Adu, n = 12. Scale bar = 750 μm. **F–I**, Thioflavin S (ThioS) staining for insoluble, fibrillar plaques (**F**) with quantification for area covered by total amyloid (**G**), parenchymal plaques (**H**), and CAA (**I**) pathology in overlaying cortex (Control IgG, n = 12; HAE-4, n = 14, chi-Adu, n = 12). Scale bar = 750 μm. **J, K**, Insoluble $Aβ_{40}$ (**J**) or $Aβ_{42}$ (**K**) protein concentrations from bulk cortical tissue lysate homogenized in guanidine measured by

ELISA and normalized to total protein concentration in cortex (Control IgG, n = 13; HAE-4, n = 14, chi-Adu, n = 12). **L–O**, Forebrain vessel isolation paradigm using dextran gradient centrifugation of a separate 5XE4 cohort treated with antibodies (**L**; Control IgG, n = 13; HAE-4, n = 12, chi-Adu, n = 13). Isolated brain vasculature fluorescently stained for $X34^{+}$ fibrillar CAA, endothelial marker CD31, and nuclei marker TOPRO3. Scale bar = 150 μm. (**M**). Insoluble $A\beta_{40}$ (**N**) and $A\beta_{42}$ (**O**) protein concentrations assessed by ELISA from forebrain-extracted vessels sonicated in guanidine-HCL and normalized to total protein concentration. Control = Control IgG. Chi-Adu = Chimeric Aducanumab. Data expressed as mean ± SEM, one-way ANOVA with Tukey's post hoc test (two-sided) performed for all statistical analyses except Kruskal-Wallis test with Dunn's multiple comparisons test (two-sided) for parenchymal Aβ/ThioS, and $A\beta_{40}$ analysis (**D, H, J**). $^{*}P < 0.05$, $^{**}P < 0.01$. No other statistical comparisons are significant unless indicated.

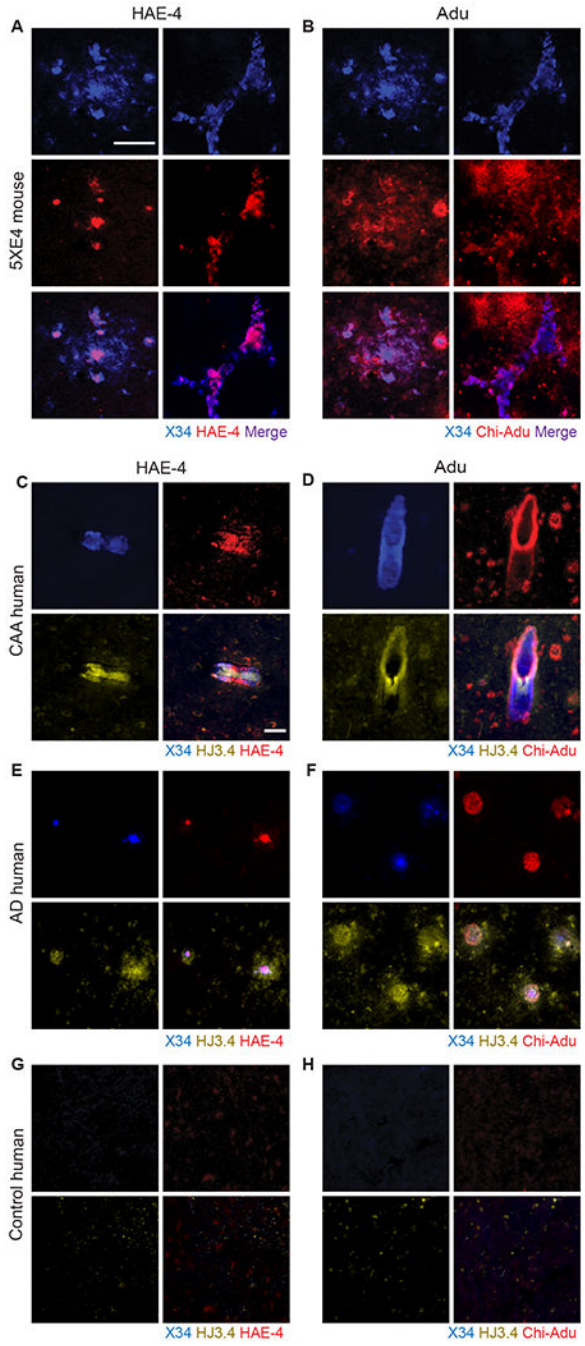

Fig. 2: HAE-4 selectively binds dense core fibrillar plaques whereas chi-Adu recognizes both dense core and diffuse Aβ plaques.

A, B, Triple co-staining of X34, HAE-4 (**A**), and chi-Adu (**B**) in unfixed, cortical tissue of a 22-month-old 5XE4 male mouse for plaque-binding profile of antibodies to either APOE (HAE-4) or Aβ (chi-Adu). Left panel in **A** and **B**: parenchymal plaque. Right panel: CAA. Scale bar = 50 μm. **C–H**, Human autopsy brain tissue from patients (n = 1 per group) including CAA (**C, D**), AD only (**E, F**), or no pathology (**G, H**) stained with X34, HJ3.4 (pan-Aβ), HAE-4, or chi-Adu. Scale bar = 50 μm. Chi-Adu = Chimeric Aducanumab.

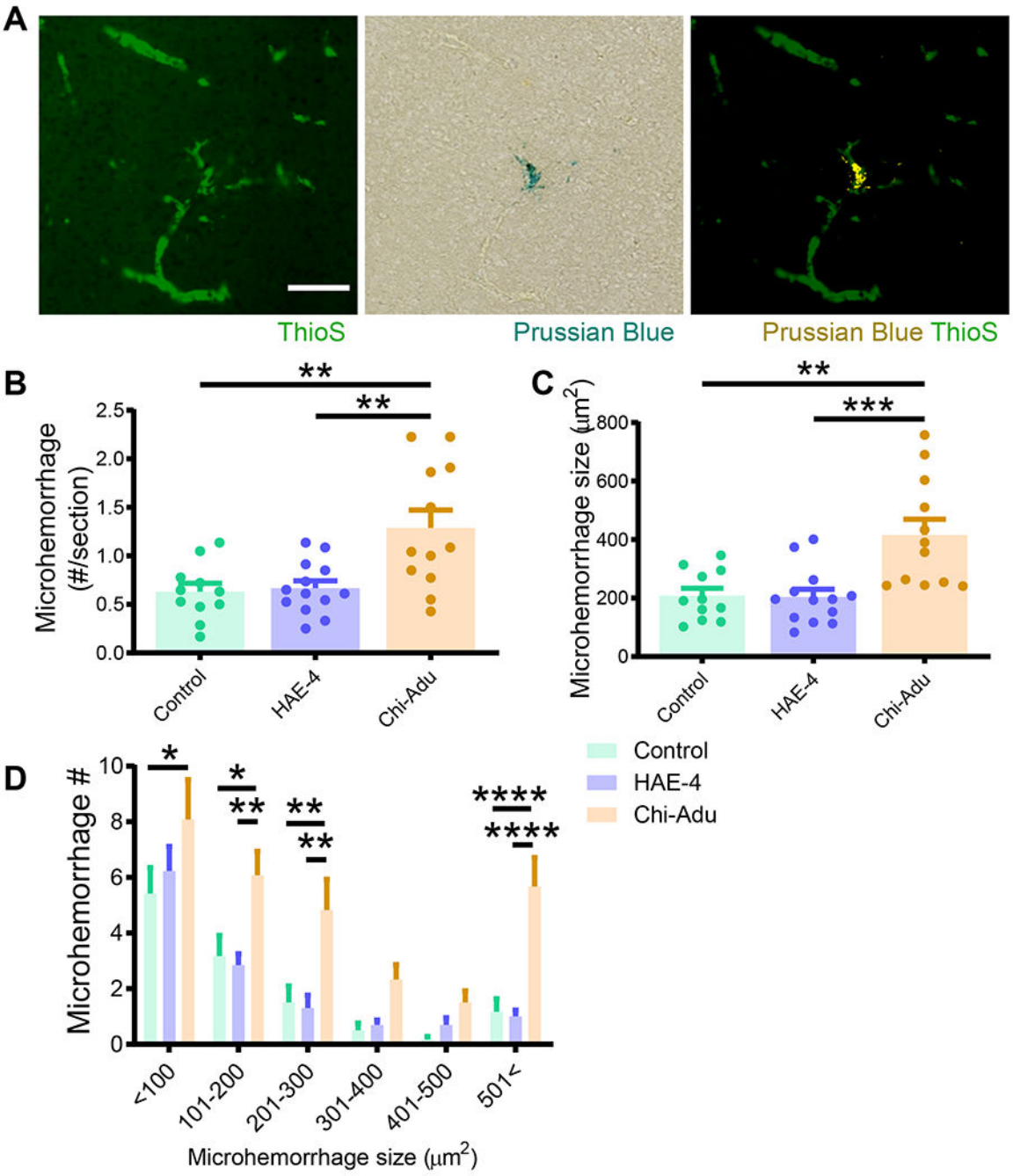

Fig. 3: Chi-Adu exacerbates CAA-associated brain microhemorrhages whereas HAE-4 does not.

A, Dual labeling of ThioS$^+$ fibrillar CAA and Prussian blue for hemosiderin deposits revealed CAA-associated microhemorrhages (right panel: microhemorrhage digitally converted to yellow) in 10-month-old 5XE4 mice. Scale bar = 100 μm. **B, C**, Prussian blue staining analysis for microhemorrhage frequency (**B**) and size (**C**) in 5XE4 mice dosed weekly for 8 weeks with antibody treatment (50 mg/kg, i.p.; Control IgG, n = 11; HAE-4, n = 13, chi-Adu, n = 12). One-way ANOVA with Tukey's post hoc test (two-sided). **D**, Number of microhemorrhages binned in 100 μm^2 increments for frequency/size distribution.

Control = Control IgG. Chi-Adu = Chimeric Aducanumab. Data expressed as mean ± SEM, two-way ANOVA with Tukey's post hoc test (two-sided). *$P < 0.05$, **$P < 0.01$, ***$P < 0.001$, ****$P < 0.0001$. No other statistical comparisons are significant unless indicated.

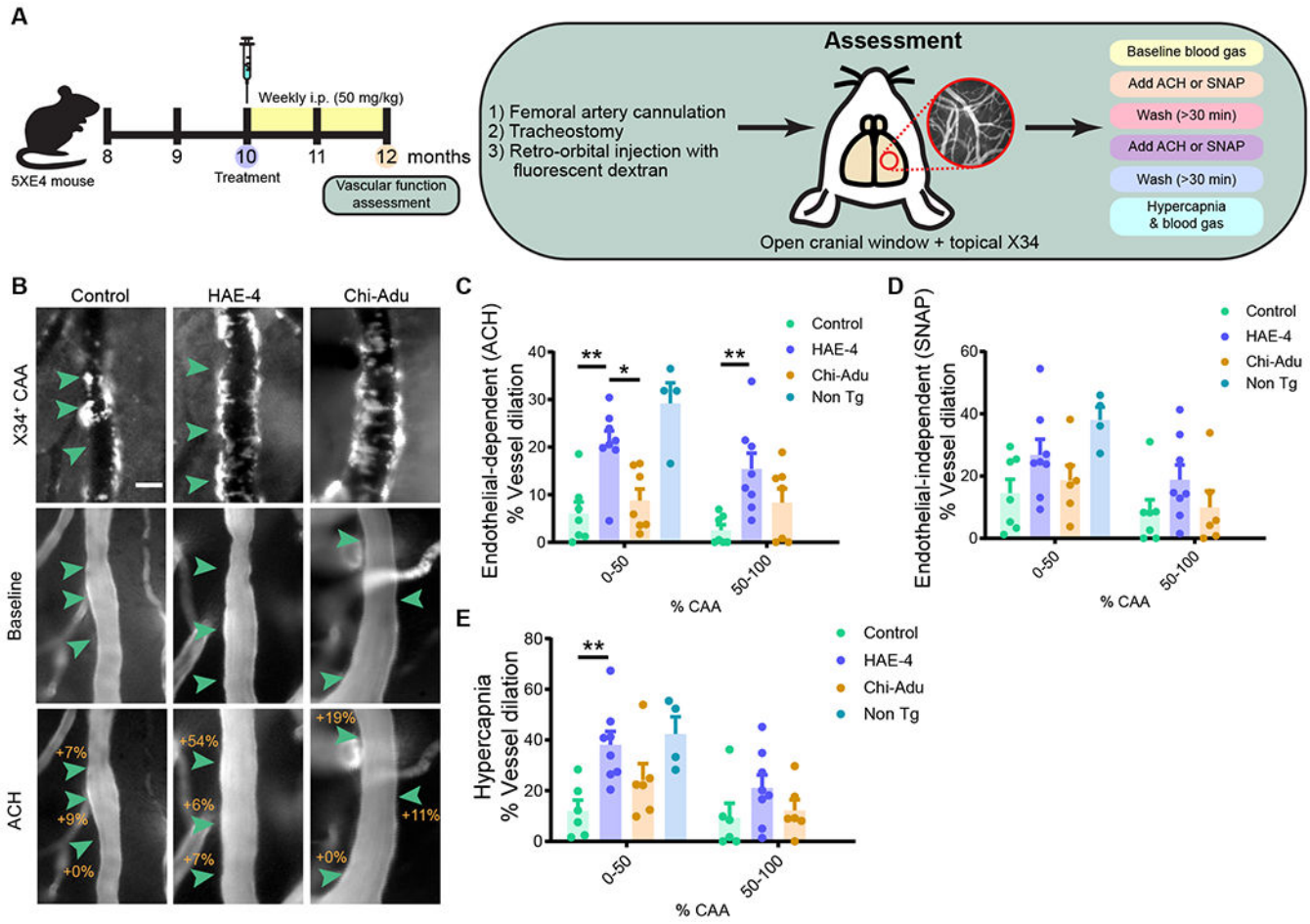

Fig. 4: HAE-4 restores vascular function to CAA-laden leptomeningeal arteries in vivo.

A, Schematic of antibody treatment and experimental design in 12-month-old 5XE4 mice for assessment of pial vascular function using endothelial-dependent ACH, vascular smooth muscle cell-dependent SNAP, and CO_2-induced hypercapnia. **B**, Representative images of $X34^+$ CAA on vessel segment at baseline or after ACH exposure. **C–E**, Percent vasodilatory change calculated at baseline and after ACH (**C**, Control IgG, n = 7; HAE-4, n = 8, chi-Adu, n = 7, Non Tg, n = 4), SNAP (**D**, Control IgG, n = 7; HAE-4, n = 8, chi-Adu, n = 6, Non Tg, n = 4), or hypercapnia (**E**, Control IgG, n = 6; HAE-4, n = 8, chi-Adu, n = 6, Non Tg, n = 4). Scale bar = 25 μm. ACH = Acetylcholine. SNAP = *S*-Nitroso-*N*-acetyl-*DL*-penicillamine. Control = Control IgG. Chi-Adu = Chimeric Aducanumab. Non Tg = Non-transgenic. Green arrowheads indicate changes in percent dilation from baseline. Data expressed as mean ± SEM, one-way ANOVA comparison with Tukey's post hoc test (two-sided) between treatment groups in vessels with less or more than 50% CAA coverage unless otherwise stated. $*P < 0.05$, $**P < 0.01$. Non-transgenic (n = 4) versus control IgG comparisons: ACH, $P < 0.001$; SNAP, $P < 0.05$; Hypercapnia, $P < 0.05$. Non-transgenic (n = 4) versus chi-Adu comparisons: ACH, $P < 0.001$; SNAP, $P = 0.097$. No other statistical comparisons are significant unless indicated or stated.

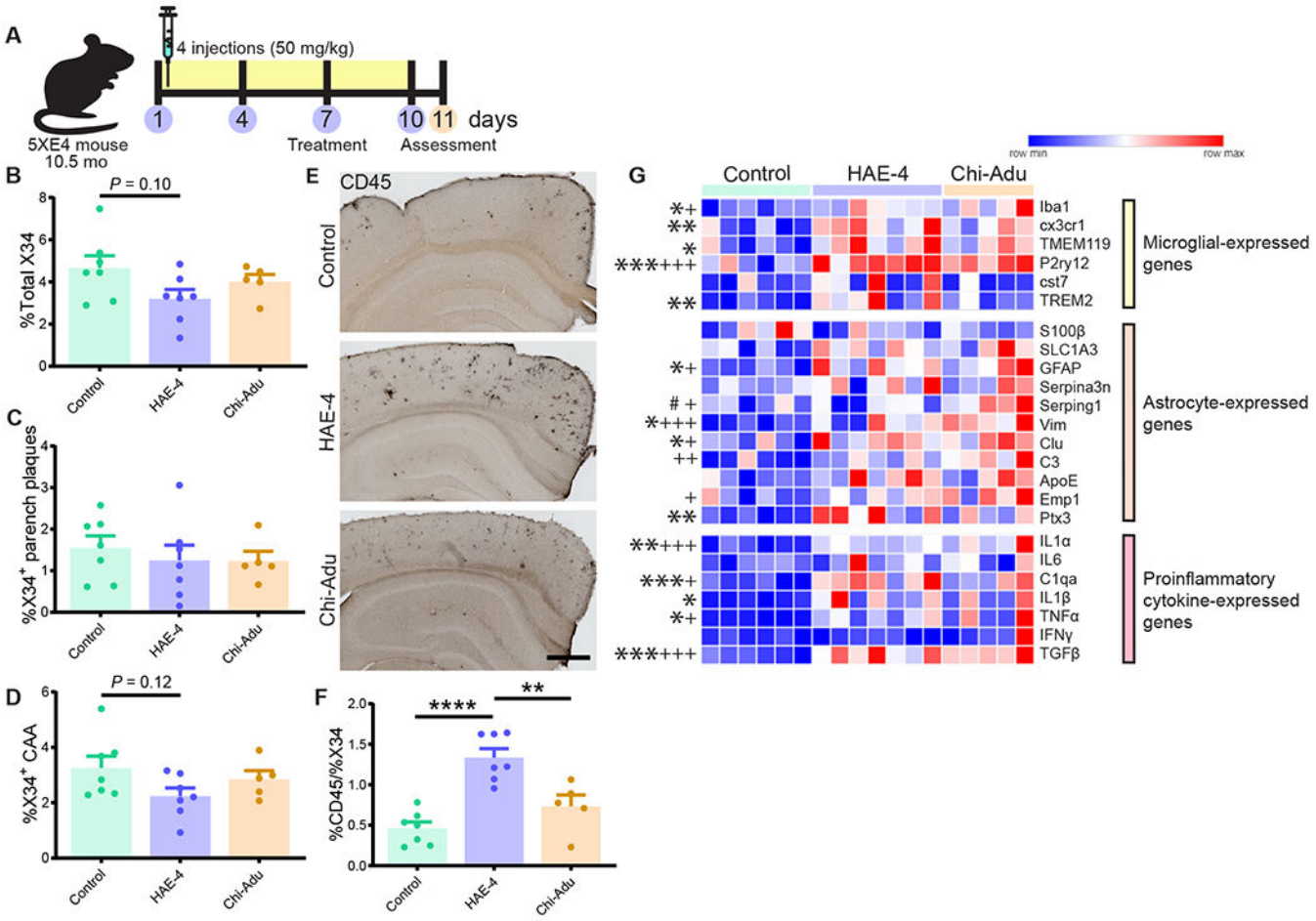

Fig. 5: Strong glial response after acute HAE-4 and chi-Adu peripheral administration.

A, Schematic design of 10.5-month-old 5XE4 mice injected once every 3 days for 4 times and assessed at 11 months-of-age. **B–D**, Quantification of total X34^{+} (**B**), parenchymal (**C**), and CAA (**D**) fibrillar plaques (Control IgG, n = 7; HAE-4, n = 7, chi-Adu, n = 5). **E, F**, CD45 (activated microglia) staining and quantification in cortex (Control IgG, n = 7 mice; HAE-4, n = 7 mice, chi-Adu, n = 5 mice). **G**, Heatmap analysis of bulk cortical microglial, astrocytic, and pro-inflammatory cytokine gene expression pattern by qPCR (Control IgG, n = 6; HAE-4, n = 7, chi-Adu, n = 5). "*" denotes statistical significance for HAE-4 versus control (*$P < 0.05$, **$P < 0.01$, ***$P < 0.001$); "+" for chi-Adu versus control ($^{+}P < 0.05$, $^{+++}P < 0.001$).; "#" for HAE-4 versus chi-Adu ($^{\#}P < 0.05$). Parench = Parenchymal. Control = Control IgG. Chi-Adu = Chimeric Aducanumab. Data expressed as mean ± SEM, one-way ANOVA with Tukey's post hoc test (two-sided). *$P < 0.05$, **$P < 0.01$, ***$P < 0.001$, ****$P < 0.0001$. No other statistical comparisons are significant unless indicated.

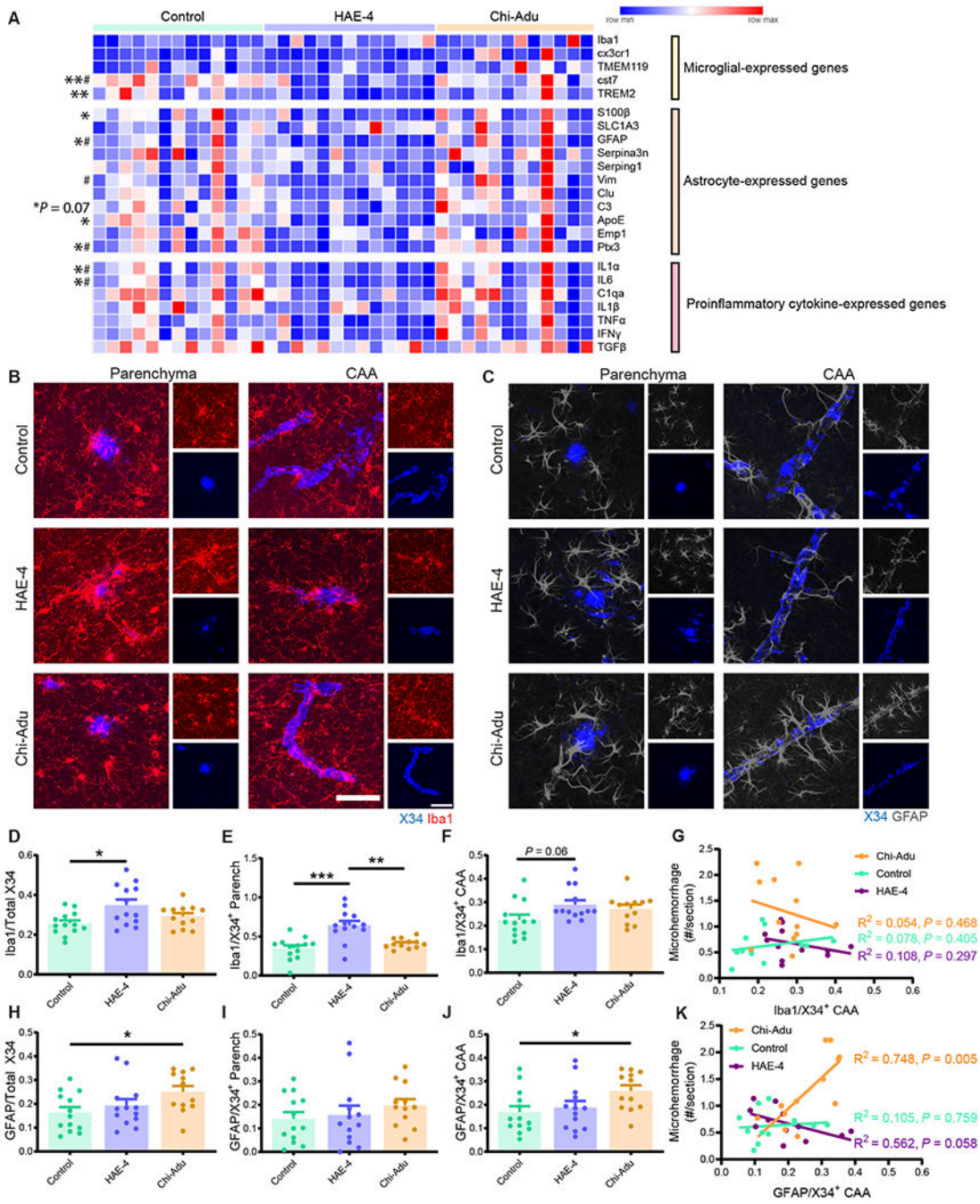

Fig. 6: HAE-4 and chi-Adu treatments stimulate differential glial responses to Aβ plaques and CAA.

A, Relative expression of microglial, astrocytic, and pro-inflammatory transcripts from bulk cortex of antibody-treated 10-month-old 5XE4 mice (50 mg/kg, weekly i.p. for 8 weeks; Control IgG, n = 13; HAE-4, n = 13, chi-Adu, n = 12) measured via qPCR, clustered by antibody treatment, and normalized to control IgG gene expression. "*" denotes statistical significance for HAE-4 versus control (*$P < 0.05$, **$P < 0.01$); "#" for HAE-4 versus chi-Adu ($^{\#}P < 0.05$). Genes analyzed using one-way ANOVA with Dunnett's multiple

comparisons test: S100β, GFAP, Vim, IL1α. One-way ANOVA with Tukey's post hoc test (two-sided) unless otherwise noted. **B–C**, Representative images of co-staining using X34 for fibrillar plaques and Iba1 for microglia (**B**) or GFAP for astrocytes (**C**) in cortex. **D–G**, Percent area of $Iba1^+$ microglia colocalized with total X34 (**D**), parenchymal (**E**), or CAA plaques (**F**), normalized to respective percent area of plaque load ($Iba1^+X34^+/X34^+$). Microglial colocalization with CAA correlated to microhemorrhage number per section (**G**; Pearson correlation: r = 0.279, R^2 = 0.078, P = 0.405, control IgG (n = 11); r = 0.329, R^2 = 0.108, P = 0.297, HAE-4 (n = 12); r = 0.232, R^2 = 0.054, P = 0.468, chi-Adu (n = 12)). **H–K**, Percent colocalization of $GFAP^+$ astrocytes and total X34 (**H**), parenchymal (**I**), or CAA plaques (**J**), normalized to respective percent area of amyloid load ($GFAP^+X34^+/X34^+$). Correlation between colocalized astrocyte/CAA and microhemorrhage number per section (**K**; Pearson correlation: r = 0.105, R^2 = 0.011, P = 0.759, control IgG (n = 11); r = 0.561, R^2 = 0.315, P = 0.058, HAE-4 (n = 12); r = 0.748, R^2 = 0.560, P = 0.005, chi-Adu (n = 12)). Large panel: Scale bar = 50 μm. Small panel: Scale bar = 50 μm. Parench = Parenchyma. Control = Control IgG. Chi-Adu = Chimeric Aducanumab. Data expressed as mean ± SEM, one-way ANOVA with Tukey's post hoc test (two-sided) for all group comparisons except Kruskal-Wallis test with Dunn's multiple comparisons test (two-sided) for data not normally distributed (**F, H,** and **I**). *P < 0.05, **P < 0.01, ***P < 0.001, ****P < 0.0001. No other statistical comparisons are significant unless indicated.